Isotope Effect and Lanthanide Contraction for 3d-4f Cyanide-Bridged Complexes Exhibiting Negative Thermal Expansion

Yusuke Kimoto, Takeshi Matsui and Takashiro Akitsu*

Department of Chemistry, Faculty of Science, Tokyo University of Science, 1-3 Kagurazaka, Shinjuku-ku, Tokyo 162-8601, Japan

Abstract: We have prepared some 3d-4f cyanide-bridged $Ln(DMF)_4(H_2O)_3Fe(CN)_6 \cdot H_2O$ complexes (Ln = Ce, Sm, Nd, and Gd; DMF = *N*,*N*-dimethylformamide) by substituting isotopes to ^2H-substituted H_2O and DMF and ^{18}O-substituted H_2O (and normal ^1H- and ^{16}O-H_2O or ^1H-DMF). We examined their crystal structures exhibiting negative thermal expansion and compared in view of hydrogen bonds and lanthanide contraction. Magnetic properties and thermal analysis exhibited importance of intermolecular hydrogen bonds in crystal lattice for this behavior. While $Fe2p_{3/2}$ and $Fe2p_{1/2}$ XAS indicated constant inner shell electron states of low-spin Fe(III) ions.

Keywords: Negative thermal expansion, cyanide, isotope, lanthanide.

INTRODUCTION

Recently, various 3d-4f molecule-based magnets such as $Ln(DMF)_4(H_2O)_3M(CN)_6 \cdot H_2O$ have been investigated widely [1, 2]. The first photo-controllable 3d-4f molecule-based magnets was $Nd(DMF)_4(H_2O)_3Fe(CN)_6 \cdot H_2O$ [3], and its crystal structure of photo-excited state was also determined [4]. Besides magnetic properties, we have systematically studied on $Ln(DMF)_4(H_2O)_3M(CN)_6 \cdot H_2O$ and related compounds in view of structure-function correlation due to lanthanide contraction and application for hybrid functional materials [5].

Previously, we found that isotope effects of temperature dependence of magnetization for $Nd(DMF)_4(H_2O)_3Fe(CN)_6 \cdot H_2O$ with ^2H-substituted H_2O and DMF ligands [6]. Since crystal structure was not determined for them, we investigated TG-DTA for intermolecular hydrogen bonds in crystal lattice and ^{57}Fe Mössbauer spectra and $Fe2p_{3/2}$ and $Fe2p_{1/2}$ XAS for coordination environment or electronic states of Fe(III) ions. The experimental results suggested that intermolecular hydrogen bonds was important for this isotope effects found in $Nd(DMF)_4(H_2O)_3Fe(CN)_6 \cdot H_2O$.

In order to discuss crystal structure directly, we examined temperature dependence of cell parameters for $Nd(DMF)_4(H_2O)_3Fe(CN)_6 \cdot H_2O$ (hereafter abbreviation of **LnFeXY** denotes Ln-Fe binuclear complexes (**LnFe**) employing ^1H_2O (**H**), ^2H_2O (**D**), and $H_2{}^{18}O$ (**O**) for **X** and ^1H-DMF (**H**) and ^2H-DMF (**D**) for **Y**) and determined crystal structures at some points. Additionally, we also compared with **CeFeXY**, **SmFeXY**, and **GdFeXY** complexes for crystal structures and several physical properties. Anisotropic negative thermal expansion [7-10] has been found for these $Ln(DMF)_4(H_2O)_3M(CN)_6 \cdot H_2O$ complexes and will be discussed novel flexibility of crystal lattices compared with previously found flexible Jahn-Teller distortion of Cu(II) complexes [11, 12].

*Address correspondence to this author at the Department of Chemistry, Faculty of Science, Tokyo University of Science, 1-3 Kagurazaka, Shinjuku-ku, Tokyo 162-8601, Japan; Tel: +81-3-5228-8271; Fax; +81-3-5261-4631; E-mail: akitsu@rs.kagu.tus.ac.jp

MATERIALS AND METHODOLOGY

General Procedure

Chemicals and solvents of the highest commercial grade available (Kanto Chemical, Tokyo Chemical Industry, and Wako) were used as received without further purification.

Preparations

$Ln(DMF)_4(H_2O)_3M(CN)_6 \cdot H_2O$ were prepared in a similar way to the analogous compounds [1, 2] by employing the corresponding metal sources and solvents substituted by the corresponding isotopes.

Physical Measurements

Infrared spectra were recorded on a JASCO FT-IR 460 plus spectrophotometer in the range of 4000-400 cm^{-1} at 298 K. Thermalanalysis (TG–DTA) was performed on a Rigaku TG8120 and α-alumina was used as the reference sample, where the heating rate was 10 K min^{-1} in the range of 313–673 K. The magnetic properties were measured with a Quantum Design MPMS-XL superconducting quantum interference device (SQUID) magnetometer at 0-50000 G at 5 K and at 5-300 K at 5000 G. The $Fe2p_{3/2}$ and $2p_{1/2}$ XAS (soft X-ray absorption spectra) were measured at KEK PF BL-19B under variable temperature. The spectra were corrected by the standard Au sample.

X-ray Crystallography

Green-yellow, yellow, or (pale) brown prismatic single crystals were glued on top of a glass fiber and coated with a thin layer of epoxy resin to measure the diffraction data. The X-ray intensities were measured at various temperature with graphite-monochromated Mo Kα radiation (λ = 0.71073 Å) on a Bruker APEX2 CCD diffractometer. The structures were solved by direct methods using SHELXS97 [13] and

1874-8465/11

expanded by Fourier techniques in a SAINT program package [14] (including SHELXTL version). The structures were refined on F^2 anisotropically for non-hydrogen atoms by full-matrix least-square methods with SHELXL97 [13]. Empirical absorption corrections were applied by a program SADABS [15]. All the non-hydrogen atoms were refined anisotropically. The hydrogen atoms were included in geometrically calculated position and refined by using riding model. The bad results in refinement are mainly due to thermal vibration of oxygen atoms of crystalline water or radiation damage.

Summary of crystallographic data of selected compounds determined complete crystal structures are as follows:

Crystallographic data for **CeFeHH** [CCDC 798466]. T = 100 K, 0.16 x 0.11 x 0.10 mm, $C_{18}H_{36}CeFeN_{10}O_8$, monoclinic, $P2_1/n$, a = 17.671(3) Å, b = 8.8685(14) Å, c = 19.605(3) Å, β = 95.059(2)˚, V = 3055.4(8) Å^3, and Z = 4, D_c = 1.558 Mgm^{-3}, μ = 2.000 mm^{-1}, R_1 = 0.0413, wR_2 = 0.1068 (3613 reflections), S = 0.777.

Crystallographic data for **CeFeHH** [CCDC 798467]. T = 150 K, 0.16 x 0.11 x 0.10 mm, $C_{18}H_{36}CeFeN_{10}O_8$, monoclinic, $P2_1/n$, a = 17.564(2) Å, b = 8.8953(10) Å, c = 19.869(2) Å, β = 95.8020(10)˚, V = 3088.4(6) Å^3, and Z = 4, D_c = 1.541 Mgm^{-3}, μ = 1.978 mm^{-1}, R_1 = 0.0340, wR_2 = 0.0938 (5364 reflections), S = 0.733.

Crystallographic data for **CeFeHH** [CCDC 798468]. T = 250 K, 0.16 x 0.11 x 0.10 mm, $C_{18}H_{36}CeFeN_{10}O_8$, monoclinic, $P2_1/n$, a = 17.594(2) Å, b = 8.9169(11) Å, c = 19.966(3) Å, β = 95.744(2)˚, V = 3116.7(7) Å^3, and Z = 4, D_c = 1.527 Mgm^{-3}, μ = 1.960 mm^{-1}, R_1 = 0.0340, wR_2 = 0.0952 (4937 reflections), S = 0.759.

Crystallographic data for **CeFeDH** [CCDC 798465]. T = 150 K, 0.34 x 0.34 x 0.23 mm, $C_{18}H_{36}CeFeN_{10}O_8$, monoclinic, $P2_1/n$, a = 17.659(2) Å, b = 8.8636(12) Å, c = 19.912(3) Å, β = 96.017(2)˚, V = 3052.8(7) Å^3, and Z = 4, D_c = 1.559 Mgm^{-3}, μ = 2.001 mm^{-1}, R_1 = 0.0303, wR_2 = 0.0921(5745 reflections), S = 0.769.

Crystallographic data for **GdFeHH** [CCDC 798469]. T = 293 K, 0.34 x 0.34 x 0.23 mm, $C_{18}H_{36}FeGdN_{10}O_8$, monoclinic, $P2_1/n$, a = 17.6109(17) Å, b = 8.8563(9) Å, c = 19.7915(19) Å, β = 96.1350(10)˚, V = 3069.2(5) Å^3, and Z = 4, D_c = 1.588 Mgm^{-3}, μ = 2.669 mm^{-1}, R_1 = 0.0552, wR_2 = 0.1576(5948 reflections), S = 1.392.

Crystallographic data for **GdFeHH** [CCDC 798470]. T = 90 K, 0.32 x 0.30 x 0.28 mm, $C_{18}H_{36}FeGdN_{10}O_8$, monoclinic, $P2_1/n$, a = 17.566(3) Å, b = 8.7966(13) Å, c = 19.483(3) Å, β = 96.281(2)˚, V = 2992.6(8) Å^3, and Z = 4, D_c = 1.628 Mgm^{-3}, μ = 2.737 mm^{-1}, R_1 = 0.0811, wR_2 = 0.2119(3574 reflections), S = 1.392.

Crystallographic data for **NdFeDD** [CCDC 798471]. T = 173 K, 0.15 x 0.10 x 0.10 mm, $C_{18}H_{36}FeN_{10}NdO_8$, monoclinic, $P2_1/n$, a = 17.5568(8) Å, b = 8.8626(4) Å, c = 19.8079(10) Å, β = 95.8720(10)˚, V = 3065.9(3) Å^3, and Z = 4, D_c = 1.561 Mgm^{-3}, μ = 2.202 mm^{-1}, R_1 = 0.0284, wR_2 = 0.0673(5887 reflections), S = 1.050.

Crystallographic data for **NdFeDH** [CCDC 798472]. T = 173 K, 0.10 x 0.10 x 0.10 mm, $C_{18}H_{36}FeN_{10}NdO_8$, monoclinic, $P2_1/n$, a = 17.5517(11) Å, b = 8.8653(5) Å, c = 19.8248(12) Å, β = 95.8370(10)˚, V = 3068.8(3) Å^3, and Z = 4, D_c = 1.560 Mgm^{-3}, μ = 2.200 mm^{-1}, R_1 = 0.0272, wR_2 = 0.0664(5995 reflections), S = 1.126.

Crystallographic data for **NdFeHD** [CCDC 798473]. T = 173 K, 0.58 x 0.18 x 0.10 mm, $C_{18}H_{36}FeN_{10}NdO_8$, monoclinic, $P2_1/n$, a = 17.5618(11) Å, b = 8.8625(6) Å, c = 19.8013(13) Å, β = 95.8800(10)˚, V = 3065.7(3) Å^3, and Z = 4, D_c = 1.561 Mgm^{-3}, μ = 2.202 mm^{-1}, R_1 = 0.0241, wR_2 = 0.0642(6221 reflections), S = 1.195.

Crystallographic data for **NdFeHH** [CCDC 798474]. T = 293 K, 0.15 x 0.09 x 0.09 mm, $C_{18}H_{36}FeN_{10}NdO_8$, monoclinic, $P2_1/n$, a = 17.615(6) Å, b = 8.906(3) Å, c = 19.934(7) Å, β = 95.966(7)˚, V = 3110(2) Å^3, and Z = 4, D_c = 1.539 Mgm^{-3}, μ = 2.170 mm^{-1}, R_1 = 0.0399, wR_2 = 0.0829(4994 reflections), S = 0.992.

Crystallographic data for **NdFeHH** [CCDC 798475]. T = 100 K, 0.15 x 0.09 x 0.09 mm, $C_{18}H_{36}FeN_{10}NdO_8$, monoclinic, $P2_1/n$, a = 17.674(2) Å, b = 8.8249(10) Å, c = 19.537(2) Å, β = 96.147(2)˚, V = 3029.6(6) Å^3, and Z = 4, D_c = 1.580 Mgm^{-3}, μ = 2.228 mm^{-1}, R_1 = 0.0323, wR_2 = 0.0676(5469 reflections), S = 1.034.

Crystallographic data for **SmFeHH** [CCDC 798477]. T = 100 K, 0.67 x 0.19 x 0.07 mm, $C_{18}H_{36}FeN_{10}O_8Sm$, monoclinic, $P2_1/n$, a = 17.649(3) Å, b = 8.8075(16) Å, c = 19.544(4) Å, β = 96.207(2)˚, V = 3020.1(10) Å^3, and Z = 4, D_c = 1.598 Mgm^{-3}, μ = 2.460 mm^{-1}, R_1 = 0.0455, wR_2 = 0.1187(5458 reflections), S = 0.862.

RESULTS AND DISCUSSION

Temperature Dependence of XAS

In general, supramolecular chemistry of crystalline materials states that non-covalent bonds such as coordination bonds and hydrogen bonds may show flexibility in crystals. We examined flexibility of crystals depending on temperature for coordination bonds (with XAS) and hydrogen bonds (with magnetic properties and TG-DTA) besides crystal structure determination.

The XAS of Fe2p$_{3/2}$ peak at 715 eV and Fe2p$_{1/2}$ peak at 725 eV were measured for **CeFeHH** at 70 and 298 K, **CeFeDH** at 30, 70, 100, 150, and 200 K, **GdFeHH** at 298 K, **GdFeDH** at 30, 65, 100, 150, 200, and 250 K, **SmFeHH** at 70 and 298 K, and **SmFeDH** at 298 K. Similar to **NdFeHH**. All data are characteristic to a low-spin Fe(III) ion. Neither isotope effect nor substitution of lanthanide ions did not affect on electronic states of Fe(III) ions in crystals.

Magnetic Properties

Magnetic properties may indicate not only superexchange interaction between Fe(III) and Ln(III) ions but also intermolecular hydrogen bonds as paths of magnetic interactions. At high temperature region, obvious discrepancy (less than the contribution of s = 1/2) due to isotope effect among **LnFeHH**, **LnFeDH**, and **LnFeOH** could be found for **Ln** = **Ce**, **Sm**, and **Gd**. Although the order of the $\chi_M T$ values at the same temperature is **GdFeHD** (> **GdFeDD** > **GdFeHH** > **GdFeDH** >) **GdFeOH**, the order is not same for **CeFe** or **SmFe**. Which suggests the reason for this differences are not electronic states of Fe(III) but intermolecular hydrogen bonds (Figs. **S1** and **S2**).

IR Spectra

Unfortunately, IR spectra exhibit little difference caused by isotope effect as O-H bands, which associate with hydrogen bonds. On the contrary, predominant bands at 2127, 2121, 2127, and 2020 cm^{-1} for **CeFe**, **NdFe**, **SmFe**, and **GdFe**, respectively, exhibit clear difference caused by metal substitution as cyanide bands.

TG-DTA

However, strength of hydrogen bonds may also vary temperature losing water molecules of isotopes, which can be detected as an endothermal peak with weight loss of TG-DTA. Actually, shift of the temperature was observed for **NdFeHH**, **NdFeHD**, **NdFeDH**, and **NdFeDD** [6]. For new compounds, the temperature was observed at 378 K for **CeFeHH**, 393 K for **CeFeDH** and **CeFeOH**, at 388K for **GdFeHH**, **GdFeDD**, and **GdFeOH** and 393 K for **GdFeDH**, and at 388 K for **SmFeHH** and 393 K for **SmFeDH**. However, the relationship between mass numbers and the temperature are not clear (Fig. **S3**) in contrast to clear differences of the temperature caused by isotope effect.

Crystal Structures

Overall crystal structures of present study are isostructural to ones reported [1, 2] and they are deposited in CCDC. Hereafter we discuss important points about negative thermal expansion only.

Fig. (**1**) exhibits temperature dependence of cell parameters for **NdFeHH**, **NdFeHD**, **NdFeDH**, and **NdFeDD**. Along the crystallographic a axis, novel anisotropic negative thermal expansion [16] was observed at 100-125 K and 125-165 K, respectively. Moreover, zero or small thermal expansion was observed at 165-210 K, and positive thermal expansion was observed at 210-250 K. The tendency of curves was same for **NdFeHH**, **NdFeHD**, **NdFeDH**, and **NdFeDD** and isotope effect resulted in slope of curves rather than the temperature. To our knowledge, this is the first report on isotope effect of negative thermal expansion associate with intermolecular hydrogen bonds [17].

By isotope effect, slight (not exactly statistical) geometrical deviation appeared at Nd1-O2 (2.429(3) Å), Fe1-C1 (1.926(4) Å), and Fe1-C3 (1.924(3) Å)) and the corresponding (hydrogen) bond distances and angles for **NdFeHH** at 173 K comparing with **NdFeHD**, **NdFeDH**, and **NdFeDD** having relatively weak hydrogen bonds. No other significant deviation could be observed for other geometric parameters. Unfortunately, complete geometries around hydrogen bonds could not be revealed even by preliminary measurements of neutron crystal structure analysis (JAEA JRR-3 BIX-3) for **NdFeDH** at room temperature. By temperature effect, **NdFeHH** at 100 K and 293 K indicates significant deviation around coordination bond of Fe1-C2 of 1.945(3) and 1.935(4) Å and cyanide ligand C2-N2 of 1.152(4) and 1.148(6) Å, respectively. By supporting other physical measurements, crystal structures show that novel anisotropic negative thermal expansion is attributed to flexible intermolecular hydrogen bonds in crystals.

Substitution of lanthanide ions resulted in similar isotope effect. For example, Ce1-O2 (2.468(3), 2.460(2), and 2.460(3) Å), Fe1-C1 (1.932(4), 1.937(3), and 1.935(4) Å), and Fe1-C3 (1.920(4), 1.937(3), and 1.934(4) Å)) at 120 K for **CeFeHH**, **CeFeDH**, and **CeFeOH**, respectively. Only the relative values of the crystallographic a axis against 100 K in important temperature region are plotted in Fig. (**2**).

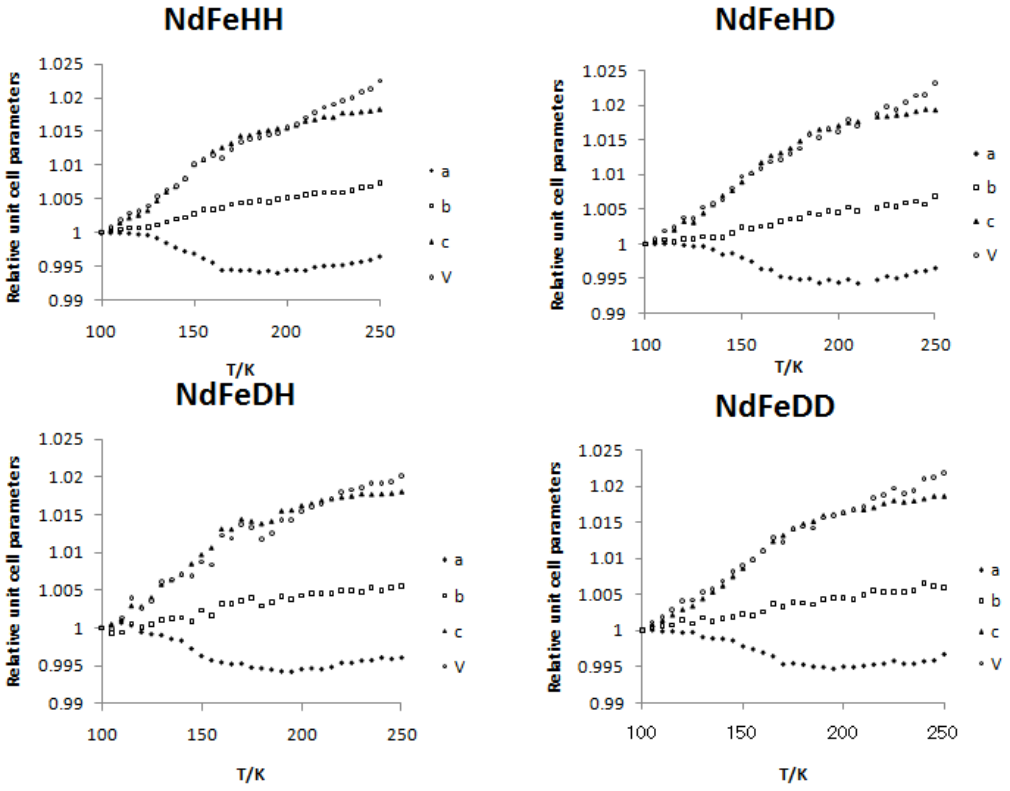

Fig. (1). Temperature dependence of cell parameters (relative values to 100 K) for **NdFeHH**, **NdFeHD**, **NdFeDH**, and **NdFeDD**.

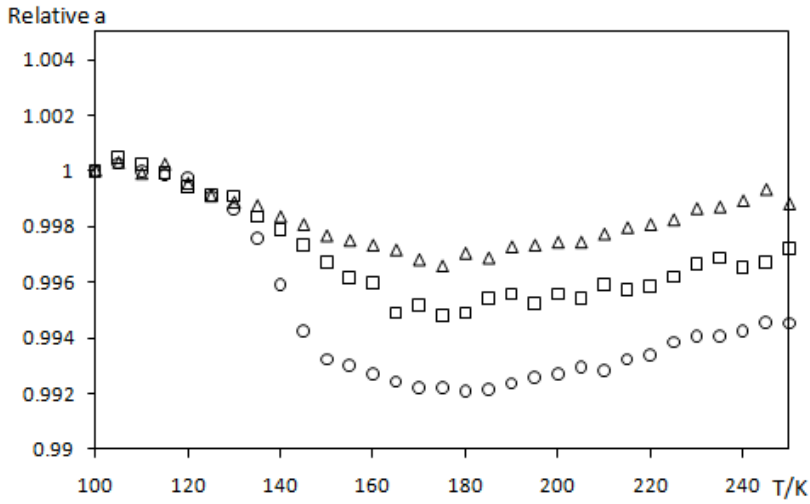

Fig. (2). Temperature dependence of the a axis (relative values to 100 K) for **CeFeHH** (circles), **SmFeHH** (squares), and **GdFeHH** (triangles).

Similar to isotope effect in Fig. (**1**), anisotropic negative thermal expansion was also observed for **CeFeHH**, **SmFeHH**, and **GdFeHH**. The slope of curves (rather than temperature) is obvious difference of negative thermal expansion by substitution of lanthanide ions.

CONCLUSION

We have successfully found negative thermal expansion for some $Ln(DMF)_4(H_2O)_3Fe(CN)_6 \bullet H_2O$ complexes. Indeed, extremely long semi-coordination bonds of Cu(II) complexes [18-22] sometimes have potential advantage to form flexible crystals against external temperature changes, which is anisotropic along the Jahn-Teller axis [23-25]. However, the present systems show anisotropically negative thermal expansion caused by not coordination bonds around lanthanide nor iron atoms but intermolecular hydrogen bonds with isotope effect for the first time.

SUPPLEMENTARY DATA

Supplementary material is available on the publishers web site along with the published article.

ACKNOWLEDGEMENTS

We are gratefully acknowledged to the Materials Design and Characterization Laboratory, Institute for Solid State Physics, the University of Tokyo for the use of the SQUID facilities and KEK-PF BL-19B (2008G528) for soft X-ray absorption spectroscopy of synchrotron radiation.

REFERENCES

[1] Figuerola A, Diaz C, Ribas J, *et al*. Synthesis and characterization of heterodinuclear Ln^{3+}-Fe^{3+} and Ln^{3+}-Co^{3+} complexes, bridged by cyanide ligand (Ln^{3+} = lanthanide Ions. nature of the magnetic interaction in the Ln^{3+}-Fe^{3+} complexes. Inorg Chem 2003; 42: 641-9.

[2] Akitsu T, Einaga Y. Structures and XPS studies of several 3d-4f cyano-bridged Ln^{III}-Fe^{III}/Co^{III} heterometallic complexes. Olyhedron 2006; 25: 2655-62; and references therein.

[3] Li G, Akitsu T, Sato O, Einaga Y. Photoinduced magnetization of the Cyano-Bridged 3d-4f heterobimetallic assembly $Nd(DMF)_4(H_2O)_3(\mu\text{-}CN)Fe(CN)_5]\cdot H_2O$ (DMF = *N*,*N*-Dimethylformamide). J Am Chem Soc 2003; 125: 12396-7.

[4] Svendsen H, Overgaard J, Chevallier M, Collet E, Iversen BB. Photomagnetic switching of the complex $Nd(dmf)_4(H_2O)_3(\mu\text{-}CN)Fe(CN)_5]\cdot H_2O$ analyzed by single-crystal X-ray diffraction. Angew Chem Int Ed 2009; 48: 2780-3.

[5] Akitsu T, Einaga Y. Structure of cyano-bridged Eu(III)-Co(III) bimetallic assembly and its application to photophysical verification of photomagnetic phenomenon. Chem Pap 2007; 61: 194-8.

[6] Akitsu T, Kimoto Y, Yamada Y, Nomura K. H/D Isotope effect and magnetic properties of cyanide-bridged Nd(III)-Fe(III) complex. Radiochim Acta (in press).

[7] Goodwin AL, Chapman KW, Kepert CJ. Guest-dependent negative thermal expansion in nanoporous prussian blue analogues $M^{II}P\text{-}t^{IV}(CN)_6\cdot x\{H_2O\}$ ($0 < x < 2$; M = Zn, Cd). J Am Chem Soc 2005; 127: 17980-1.

[8] Goodwin AL, Kennedy BJ, Kepert CJ. Thermal expansion matching *via* framework flexibility in Zinc dicyanomellates. J Am Chem Soc 2009; 131: 6334.

[9] Goodwin AL, Calleja M, Conterio MJ, *et al*. Colossal positive and negative thermal expansion in the framework material $Ag_3[Co(CN)_6]$. Science 2008; 319; 794-7.

[10] Korcok JL, Katz MJ, Leznoff DB. Impact of metallophilicity on "Colossal" positive and negative thermal expansion in a series of isostructural dicyanometallate coordination polymers. J Am Chem Soc 2009; 131: 4866-71.

[11] Falvello LR, Jahn-Teller effects in solid-state co-ordination chemistry. J Chem Soc Dalton Trans 1997; 4463-75.

[12] Halcrow MA. Interpreting and controlling the structures of six-coordinate copper(II) centres – When is a compression really a compression? Dalton Trans 2003; 4375-84.

[13] Sheldrick GM. A short history of SHELX. Acta Crystallogr A 2008; 64: 112.

[14] Bruker . SMART and SAINT. Bruker AXS Inc., Madison, Wisconsin, USA, 1998.

[15] Sheldrick GM. SADABS. Program for empirical absorption correction of area detector data, University of Gottingen, Germany, 1996.

[16] Haas S, Batlogg B, Besnard C, Schiltz M, Kloc C, Siegrist T. Large uniaial negative thermal expansion in pentacene due to steric hindrance. Phys Rev B 2007; 76: 205203.

[17] Fisher SJ, Helliwell JR. An inivestigation into structural changes due to deuteration Acta Crystallogr A 2008; 64: 359-67.

[18] Sereda O, Stoeckli-Evans H, Dolomanov O, Filinchuk Y, Pattison P. Transformation of a chiral nanoporus bimitallic cyano-bridged framework triggered by dehydration/rehydration. Crystal Growth Des 2009; 9: 3168-78.

[19] Sereda O, Neels A, Stoeckli F, Stoeckli-Evans H, Filinchuk Y. Sponge-like reversible transformation of a bimetallic cyanometallate polymer. Crystal Growth Des 2008; 8: 2307-11.

[20] Sereda O, Neels A, Stoeckli F, Stoeckli-Evans H. Chiral bimetallic assemblies and coordination polymers based on tetracyanonickelate:

a striking reversible structural transformation. Crystal Growth Des 2008; 8: 3380-4.

[21] Akitsu T, Einaga Y. Extremely long axial Cu-N bonds in chiral one-dimensional zigzag cyanide-bridged Cu^{II}-Ni^{II} and Cu^{II}-Pt^{II} bimetallic assemblies. Inorg Chem 2006; 45: 9826-33.

[22] Akitsu T, Einaga Y. Tuning of electronic properties of one-dimensional cyano-bridged Cu^{II}-Ni^{II}, Cu^{II}-Pd^{II}, and Cu^{II}-Pt^{II} bimetallic assemblies by stereochemistry of ligands. Inorg Chim Acta 2008; 361: 36-42.

[23] Akitsu T, Einaga Y, Yoza K. Thermally-accessible lattice strain and local pseudo jahn-teller distortion in various dimensional Cu^{II}-M^{III} bimetallic cyanide-bridged assemblies. Open Inorg Chem J 2008; 2: 1-10.

[24] Akitsu T, Einaga Y. Thermal and photo-responsibiliry of axial semi-coordination bonds in Copper(II) complex. Bull Chem Soc Jpn 2004; 77: 763-4.

[25] Akitsu T, Sano K. Analogy of van't Hoff relationship for thermally-accessible lattice strain of Copper(II) complex. Netsu Sokutei 2009; 36: 244-6.

Received: October 29, 2010 Revised: January 25, 2011 Accepted: January 27, 2011